

Listric versus planar normal fault geometry: an example from the Eisenstadt-Sopron Basin (E Austria)

Darko Spahić · Ulrike Exner · Michael Behm ·
Bernhard Grasemann · Alexander Haring ·
Herbert Pretsch

Received: 26 October 2009 / Accepted: 28 July 2010 / Published online: 13 August 2010
© Springer-Verlag 2010

Abstract In a gravel pit at the eastern margin of the Eisenstadt-Sopron Basin, a satellite of Vienna Basin (Austria), Neogene sediments are exposed in the hanging wall of a major normal fault. The anticlinal structure and associated conjugated secondary normal faults were previously interpreted as a rollover anticline above a listric normal fault. The spatial orientation and distribution of sedimentary horizons and crosscutting faults were mapped in detail on a laser scan of the outcrop wall. Subsequently, in order to assess the 3D distribution and geometry of this fault system, a series of parallel ground penetrating radar (GPR) profiles were recorded behind the outcrop wall. Both outcrop and GPR data were compiled in a 3D structural model, providing the basis for a kinematic reconstruction of the fault plane using balanced cross-section techniques. However, the kinematic reconstruction results in a geologically meaningless normal fault cutting down- and up-section. Additionally, no evidence for a weak layer serving as ductile detachment horizon (i.e. salt or clay horizon) can be identified in stratigraphic profiles. Instead, the observed deflection of stratigraphic horizons may be

caused by a displacement gradient along a planar master fault, with a maximum displacement in the fault centre, decreasing towards the fault tips. Accordingly, the observed deflection of markers in the hanging wall—and in a nearby location in the footwall of the normal fault—is interpreted as large-scale fault drag along a planar fault that records a displacement gradient, instead of a rollover anticline related to a listric fault.

Keywords Listric fault · Fault drag · Ground penetrating radar · Balanced cross-section

Introduction

Listric faults or shovel-shaped faults (Suess 1909) are defined as curved normal faults in which the dip decreases with depth resulting in a concave upwards shape (e.g. Bally 1983; Shelton 1984). Two features are considered as characteristic of listric normal faults (Wernicke and Burchfiel 1982): (1) a steep upper part of the normal fault flattening downwards or merging with a low-angle detachment and (2) the down-warping or reverse drag (Hamblin 1965) of the hanging wall block forming a roll-over anticline. Investigations into the origin of this wide-spread phenomenon that is very often used as a tool in hydrocarbon explorations (Tearpock and Bischke 2003 and references therein) are predominantly focused on the importance of fault shape. Broadly, two kinematic groups of rollover systems appear common: fault rollovers induced by extensional displacement along a listric fault shape and expulsion rollovers developed because of salt withdrawal (e.g. Ge et al. 1997; Krézsek et al. 2007; Brun and Mauduit 2008, 2009). Kinematic and geometric balancing techniques of extensional rollover anticlines

D. Spahić (✉) · U. Exner · B. Grasemann · H. Pretsch
Department for Geodynamics and Sedimentology,
University of Vienna, Althanstrasse 14,
1090 Vienna, Austria
e-mail: darko.spahic@univie.ac.at

M. Behm
Institute of Geodesy and Geophysics,
Vienna University of Technology,
Gusshausstrasse 27-29, 1040 Vienna, Austria

A. Haring
Christian Doppler Laboratory for “Spatial Data from Laser
Scanning and Remote Sensing”, Vienna University of
Technology, Gusshausstrasse 27-29, 1040 Vienna, Austria

provided reconstructions of the depth of an underlying detachment horizon (Chamberlin 1910; Wernicke and Burchfiel 1982; Tearpock and Bischke 2003). The understanding of the geometric evolution of listric fault systems was significantly improved by employing scaled analogue models (e.g. McClay 1990; McClay and Scott 1991; Xiao and Suppe 1992; Yamada and McClay 2003; Dooley et al. 2003) and more recently numerical models (Crook et al. 2006). Analogue models comprise a deformable hanging wall, composed of unconsolidated sand that is extended over a rigid footwall block (Yamada and McClay 2003). By employing rigid footwall blocks, the geometry of the master fault is predefined by the footwall block shape and remains fixed throughout the deformation history. However, some authors suggested that footwall deformation or collapse could be important mechanisms during extension along listric faults (Gibson et al. 1989; Brun and Mauduit 2008; Krézsek et al. 2007), which are inherently neglected in analogue models or balancing techniques assuming a rigid footwall. Based on mechanical arguments, the common assumption that a hanging wall rollover anticline automatically implies a listric fault geometry (e.g. Shelton 1984; Yamada and McClay 2003) was questioned by several authors (e.g. Barnett et al. 1987; Mauduit and Brun 1998; Grasemann et al. 2005; Brun and Mauduit 2008). Alternatively, reverse drag of strata both in the hanging wall and in the footwall may develop around a planar fault surface, where the displacement decreases towards the fault tips (e.g. Barnett et al. 1987; Gupta and Scholz 1998; Mansfield and Cartwright 2000).

In this study, we investigate a normal fault system in a south-eastern satellite basin of the Vienna Basin (Austria), where tilting of sediments close to the fault was previously interpreted as a rollover anticline associated with a listric fault geometry (Decker and Peresson 1996). This paper focuses on the exposed hanging wall of the normal fault, comprising (1) field mapping supported by terrestrial laser scanning of the outcrop (2) GPR imaging of the deformed sediments and (3) geometric reconstruction of the fault geometry by coulisse cross-section balancing. An integrated structural model is used to discuss the plausibility of a listric normal fault.

Regional setting

The Vienna Basin, located between the Alpine- and the Carpathian mountain belt, formed in the Miocene as a result of the lateral extrusion of the Eastern Alps (Royden 1985; Ratschbacher et al. 1991). Mostly, SW–NE trending transpressive strike-slip and normal faults permitted the deposition of up to 5,000 m of marine to lacustrine sediments in the centre of the basin from the Carpathian fold

belt and Pannonian basin (e.g. Fodor 1995). The multi-staged tectonic evolution started with a piggyback basin in the Lower Miocene positioned on the top of Alpine advancing thrust sheets (Wagreich, 2000), followed by a pull-apart stage in the Middle to Upper Miocene. After a Pannonian basin inversion phase, E–W extension lasted at least until the Pleistocene (Decker 1996) and is probably still active (Chwatal et al. 2005; Decker et al. 2005; Hinsch et al. 2005). The basin was extensively studied for hydrocarbon exploration (Wessely 1988; Strauss et al. 2006).

In the south-east, the Vienna Basin is connected to the Eisenstadt-Sopron Basin which is a small satellite basin with 2,000 m of sediment infill. The economically less important and thus less explored basin is bordered by normal faults (Fig. 1) and experienced its main subsidence phase in the Badenian (Schmid et al. 2001). The eastern margin of the basin is defined by the N–S trending Köhida normal fault system (Fodor 1995).

The investigated outcrop (Fig. 2) is situated at the eastern margin of the Eisenstadt-Sopron basin, along a NNE–SSW striking normal fault, a part of the Köhida fault system, displacing Badenian calcareous silt in the East against a succession of Sarmatian and Pannonian gravels and calcareous sands in the West (Harzhauser and Kowalke

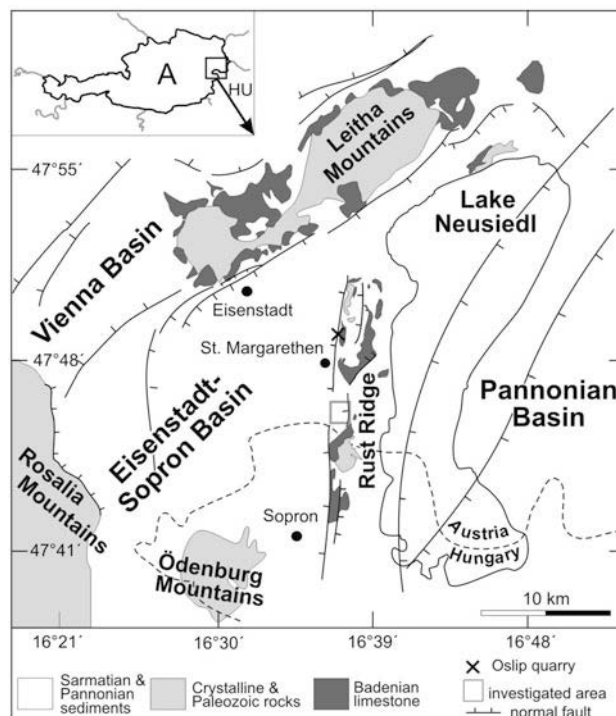


Fig. 1 Tectonic sketch map of the Eisenstadt-Sopron Basin (eastern Austria). The investigated gravel pit is located on the eastern basin margin, 5 km south of the village St. Margarethen. A normal fault (referred to as master fault in the text) juxtaposes Badenian silts and limestone in the E with Sarmatian and Pannonian gravels and sands in the W (modified after Schmid et al. 2001)

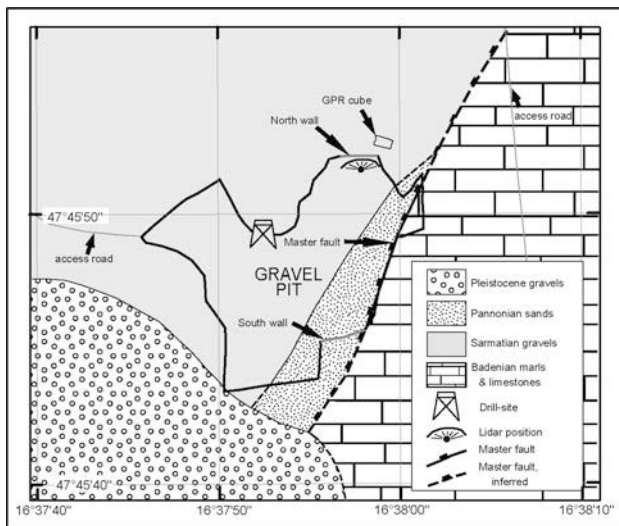


Fig. 2 Detailed map showing the investigated outcrop walls and GPR location in the gravel pit and the surrounding geology. The master fault juxtaposes Badenian marls and limestones in the E with Sarmatian and Pannonian gravels and sands

2002). In the southern part of the investigated area, both footwall and hanging wall sediments are covered by Pleistocene gravels, which post-date the activity of the normal fault. Approaching the fault plane, the hanging wall strata record an increase in dip angle from West to East, which was interpreted as rollover anticline associated with a listric normal fault by Decker and Peresson 1996.

Data acquisition, processing and results

The investigated outcrop is located inside a gravel pit situated ca. 5 km south of the village St. Margarethen, Burgenland, Austria (Fig. 1). A WNW-dipping normal fault (referred to as master fault in the following text) was mapped along the eastern margin of the pit (Decker and

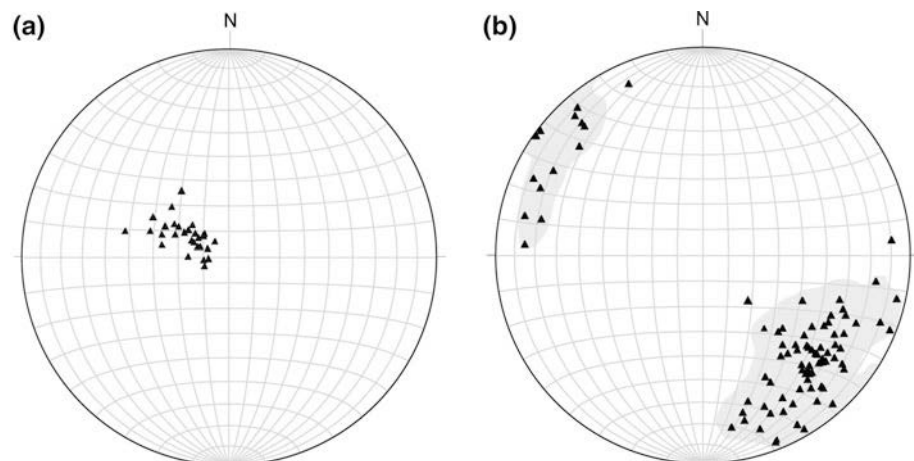
Peresson 1996). While the footwall of the master fault consisting of Badenian sediments is hardly exposed, the hanging wall comprising a sequence of middle Miocene (Sarmatian and Pannonian) gravels, silts and sands (Harzhauser and Kowalke 2002) can be studied in detail. The sedimentary beds are tilted up to ca. 35° towards the master fault, forming an anticlinal structure in the hanging wall of the master fault (Fig. 3a). Additionally, several smaller normal faults with variable length and displacement, oriented sub-parallel and conjugate to the master fault, crosscut the sedimentary beds (Fig. 4b). In order to generate a 3D structural model and constrain the geometry and kinematics of the master fault, the following methods were applied: (1) detailed structural measurements of the sedimentary layers and the exposed faults, (2) terrestrial laser scanning to obtain a high-resolution digital surface model and georeferenced, rectified image of the outcrop wall, (3) GPR survey behind the scanned wall to image the unexposed 3D geometry of the sedimentary beds and faults and (4) 2D section balancing to reconstruct the geometry of the proposed listric normal fault at depth. Combining these datasets, we generated a 3D structural model of the normal fault and the deformed hanging wall sediments.

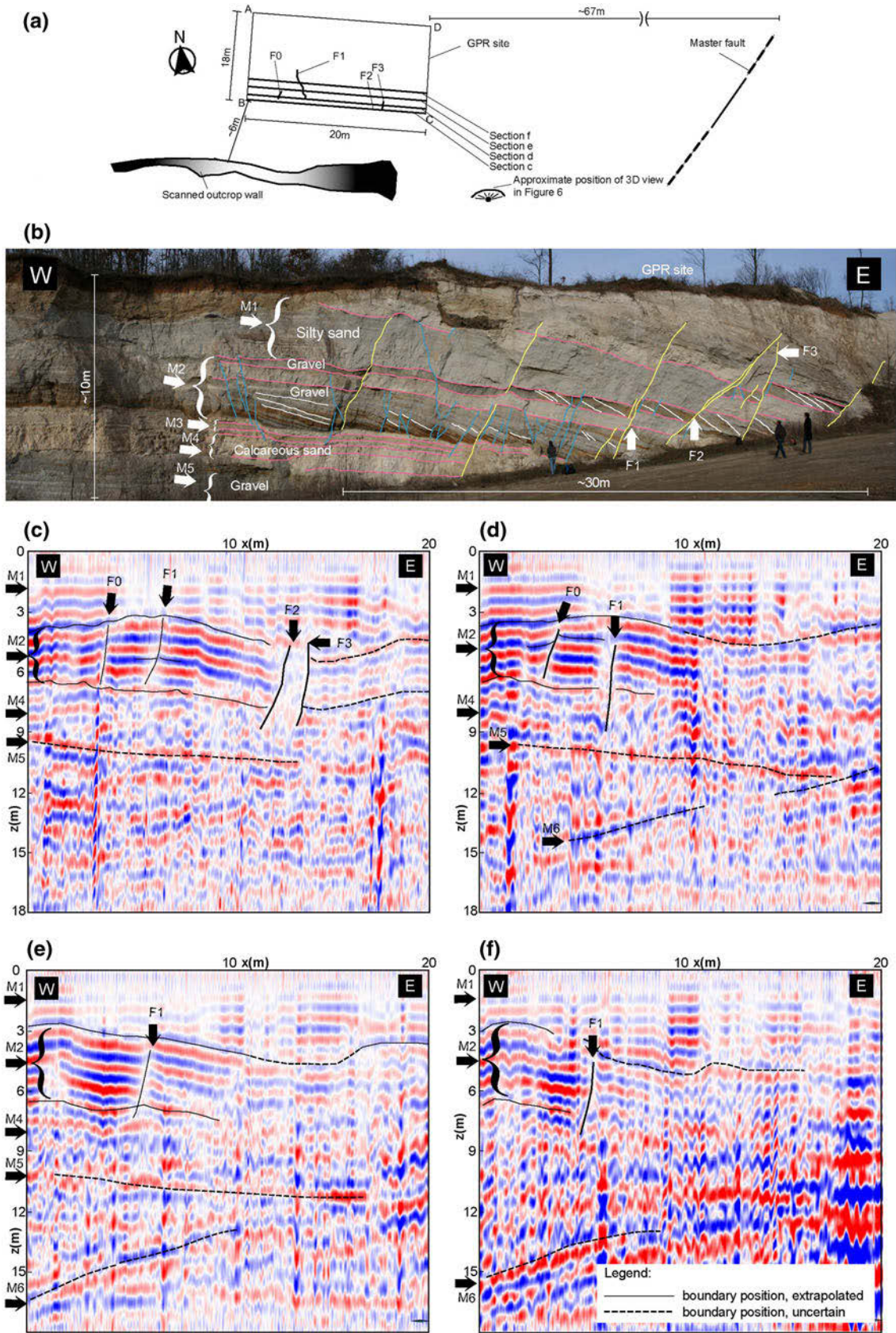
Structural data

The investigated outcrop is located at the north-eastern margin of the gravel pit, where a 10-m-high and 30-m-wide E–W oriented wall exposes the Sarmatian-Pannonian succession in the hanging wall of the master fault (Fig. 2).

We identified five characteristic marker units (M1–M5 in Fig. 4b) in the exposed section which were later used for correlation with horizons mapped in the GPR data. The top of the exposure is represented by a fine-grained silty sand and silt of 2 m thickness (M1). Below, two medium to coarse-grained cross-bedded sandy gravel horizons, with

Fig. 3 Equal area projections, lower hemisphere: **a** poles to bedding planes (29) and **b** poles to fault planes (90), max. value: 16.2% at 311/62, contours at: 1.20 measured along the northern wall





◀ **Fig. 4** **a** Map view of the investigated site, depicting the position of the scanned outcrop wall and the location of the GPR site; **b** Geological interpretation of the investigated wall, identifying the marker horizons (M1–M5), faults (marked in yellow) and deformation bands (blue); **c–f** GPR sections N of and roughly parallel to the outcrop wall. Profile c is at ca. 6 m distance from the wall, the distance between the individual profiles is between 0.5 and 1.5 m as indicated in **a**. Variations in reflection intensity are interpreted as marker horizons, i.e. variation in lithological composition, most of which can be traced in all four sections. Sub-vertical offsets in the GPR signal can be correlated with larger fault structures; the fault F1 is observed in all sections, while the signals of F1 and F3 are lost further to the N

one intercalated bed of yellowish calcareous sand, are summarized as a 4-m-thick M2 marker. The grey-brownish coloured gravel beds comprise planar beds (visible in the W part of the section, Fig. 4), as well as foreset beds dipping 12° steeper to the E than the planar beds. A distinctive, 0.1-m-thick layer of marly silt containing ca. 40% gastropod shells (*Granulolabium Bicinctum*, Harzhauser and Kowalke 2002) is marked as M3, which was used as reference horizon in two parallel profiles along the northern and southern margin of the gravel pit for 2D section balancing. The base of the exposed section is composed of another moderately cemented, yellowish calcareous sand of 3-m-thickness (M4), and a grey gravel horizon (M5) predominated by planar beds with an undefined thickness due to lack of exposure. One additional marker (M6) comprising mainly coarse gravel and intercalated sand beds was identified in deeper sections of the gravel pit but is not exposed on the investigated outcrop wall.

Along the outcrop, the dip of the planar sedimentary layers increases gradually from W to E, with a dip towards the E of 8° in the W to a maximum of 34° in the E. This anticlinal structure was earlier interpreted as an expression of hanging wall collapse above a listric normal fault (Decker and Peresson 1996). In detail, the increase of dip is not only related to a gentle folding, but dip variations occur abruptly at secondary normal faults oriented parallel and at a conjugate angle to the master fault (Fig. 4b). Most of the observed faults are more accurately described as deformation bands (Exner and Grasemann 2010), restricted to the lower gravel in M2 and displacing the sedimentary layering only some few centimetres. These small faults record a displacement gradient from the centre towards the tips, which promotes the development of reverse drag in the adjacent sedimentary layers (Hamblin 1965; Grasemann et al. 2005). Propagation and rotation of some faults lead to vertical coalescence and the generation of faults with larger offset up to a maximum of 4 m, crosscutting the entire exposed section. As all of the observed long faults cut across sedimentary horizons with a documented hiatus of several thousands of years (Harzhauser and Kowalke 2002), and no increase in thickness of the Sarmatian beds

towards the master fault is documented, a syndimentary generation of these faults can be ruled out.

Borehole data from a groundwater exploration drilling, located inside the gravel pit ca. 100 m SW of the outcrop wall (marked in Fig. 2), do not provide any indication of a possible detachment horizon, i.e. salt or silt, down to a depth of 20 m below the exposed section. Instead, the succession of Sarmatian gravels and sands continues without any notable disturbances.

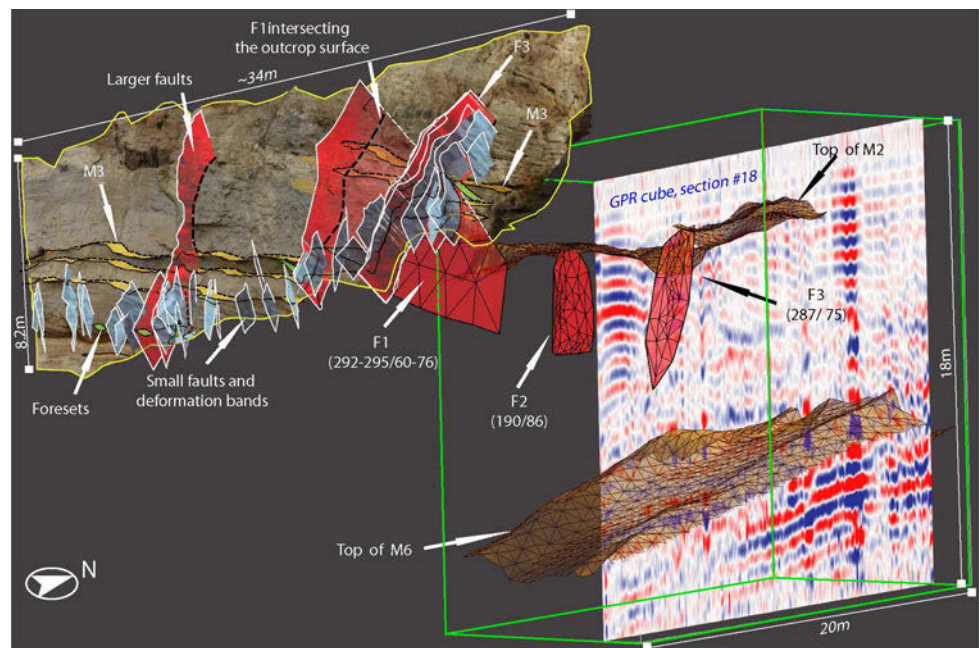
Ground penetrating radar

Ground penetrating radar (GPR) is commonly employed for detecting near surface geological features in sediments (e.g. Bristow and Jol 2003). Furthermore, several recent studies document the applicability of this method for the detection of faulted sedimentary horizons in the shallow sub-surface. Meschede et al. (1997) observed the tectonic surfaces and rollover structures associated with faults in Middle Triassic limestone of SW Germany along 2-D profiles. The hanging wall of active faults was visualized in the Betic Cordillera (Reiss et al. 2003) with high-frequency antennas. To infer the active Markgrafneusiedel Fault in shallow Pleistocene deposits and to correlate it with the deeper fault levels of the Vienna Basin, 2-D GPR profiling was applied using both low and high frequencies (Chwatal et al. 2005).

A dense network of parallel GPR profiles provides the opportunity to image sedimentary horizons and faults in the prolongation along strike N of the exposed section. The investigated site was a 20 m × 19 m sized area (Fig. 4a). Though several antennae frequencies were applied and tested, we restrict the interpretation to the best results obtained with a centre frequency of 40 MHz. The raw data are of moderate quality and gain significance by a simple but effective signal processing (background removal, bandpass filtering 15–80 MHz, weak smoothing). There is a low signal to noise ratio (S/N ratio) in the raw recordings. The reason for this remains unclear since disturbing surface features are absent, and the soil was rather dry. However, strong reverberations suggest the presence of fluids. We interpret that although the extensive tree cover was recently removed, the still existing roots contain a relatively high amount of water.

Forty-one 40-MHz GPR sections were collected along 20-m-long, E–W oriented lines with a relative spacing of 0.5 m. The sections are parallel to the exposed wall and perpendicular to the N–S striking faults. Assuming a propagation velocity of 0.12 m/ns (Bristow and Jol 2003), the signal penetration depth is approximately 15 m. The processed GPR sections were interpolated into a depth converted cube such that sections with arbitrary directions can be visualized. Since the topography is rather flat and even, no topographic correction was applied.

Fig. 5 Three-dimensional structural model constructed from the rectified outcrop image draped on terrestrial laser scan (TLS) data and the ground penetrating radar (GPR) cube (in the background). No vertical exaggeration. The exposed fault and horizon surfaces are constructed in great detail, accurately respecting the dip and dip direction of each element. Selected fault and horizon surfaces mapped from GPR data are connected to the outcrop structures (e.g. F1)



Four representative GPR profiles striking parallel to the outcrop wall (Fig. 4a) are presented in (Fig. 4c–f). The strong reflections, located between 3 and 6 m below the surface, can be correlated with the M2 gravel horizons identified in the outcrop section. Below, the marker horizons M4, M5 and M6 can be tentatively assigned to single high reflectors in the individual sections. Most reflectors slightly dip towards the E or show an undulating geometry. Abrupt disturbances, representing a lack of energy in an otherwise continuous reflection band, are interpreted as faults. Some faults (e.g. F1) can be identified in several sections, thus providing additional constraints on their strike direction (Fig. 4a). The 40-MHz antenna did not depict smaller-sized faults mapped in the outcrop, which have less than 3 m in length and correspondingly only some centimetres or decimetres of displacement. Finally, another strong reflector M6, which is not exposed at the nearby outcrop wall, was recorded in most 40-MHz GPR sections. This horizon, approximately 17 m below surface (and ~ 7 m below the base of the exposed wall) conspicuously dips in the opposite direction to the upper reflectors, i.e. 25° to the SW.

Laser scan and 3D model

We used a terrestrial laser scan (TLS) system (RIEGL LMS-Z420i), consisting of a high-performance long-range 3D laser scanner and a calibrated high-resolution digital camera mounted onto the scanner head, to generate a digital surface model and a rectified image of the investigated outcrop wall. The entire wall and the surroundings were scanned from a single point, which was recorded

using a differential global positioning system receiver (DGPS). The point-cloud of xyz-coordinates acquired by TLS was imported into Gocad, a three-dimensional visualization software, and the points corresponding to the outcrop wall were meshed to form a virtual outcrop surface, onto which the rectified image was draped (McCaffrey et al. 2005). By integrating the measurements of the respective bedding and fault planes, a 3D structural model of the outcrop data was generated (Fig. 5), taking account of the exact location and orientation of the structural features. To compare the structural measurements collected at the outcrop wall with the GPR imaging results, we integrated both datasets into the 3D model, providing the framework for the further structural interpretation.

Apart from digitizing numerous faults along the outcrop wall, three distinctive fault surfaces were additionally mapped in the GPR dataset. Although the outcrop wall is located at a rather large distance (ca. 6 m) from the closest GPR section, we were able to connect the fault traces from the GPR sections with three of the larger faults in the outcrop and construct strike and dip of the fault planes. Similarly, the well-traceable marker horizons M2 and M6 were connected to horizon surfaces in the structural model (Fig. 5).

Depth to detachment construction assuming a listric fault geometry

A great number of geometrical reconstructions of extensional faults have been proposed and discussed by several authors (e.g. Davison 1986; Williams and Vann 1987; White 1992; Yamada and McClay 2003). Most of these models are based

on the geometric relationships between the hanging wall structures and the underlying detachment using vertical, oblique or flexural slip restoration assuming either conservation of the area/bed-length on a cross-section and/or constant slip along the fault (for a discussion of models with area change and slip gradients see Wheeler 1987). All these models have in common that sediments in the hanging wall above a rigid fault surface with a listric geometry deform into a rollover anticline, while the footwall remains undeformed (Tearpock and Bischke 2003 and references therein). Comparing different reconstruction techniques with a positive inversion analogue experiment, Yamada and McClay (2003) suggested that the inclined simple shear model most accurately approximates the restoration of the hanging wall deformation. This technique assumes that deformation of the hanging wall occurs by simple shear along inclined slip planes that are either parallel to syn- or antithetic faults (White et al. 1986; Dula 1991). The shear angle of these faults is frequently estimated using the Mohr–Coulomb Theory resulting in dip angles between 60° and 70° (Tearpock and Bischke 2003). In order to reconstruct the master fault geometry from a hanging wall rollover anticline, the heave of a marker horizon must be known. The bed thicknesses along the shear planes remain fixed, and therefore this technique always results in a hanging wall area-balanced reconstruction. Practically, the marker horizon is divided into domains of constant dip, and the amount of displacement between the dip domains is defined by the distance along the plane between the reconstructed and the deformed geometry of the marker horizon.

Being aware of the limitations of geometrical reconstructions, we used the inclined simple shear model in order to reconstruct the depth of the detachment, assuming that a rigid listric fault forced the deformation of the marker horizon M3 of the northern and southern pit walls in St. Margarethen (Fig. 2). The most sensitive parameter, which

strongly influences the location and the orientation of the detachment, is actually the spatial position constrained by the widths and orientations of the dip domains with respect to the orientation of the fault plane containing the hanging wall cut-off of the marker horizon. Therefore, the dip domains were constructed as accurately as possible using the 3D structural model including the exposed sections of M3 as well as its spatial orientation in the sub-surface. According to the mean of the measured fault planes in the hanging wall (Fig. 3b), the dip of the inclined shear planes is 72° . The fault plane containing the hanging wall cut-off of the marker horizon M3 dips 60° towards WNW. Our depth to detachment calculations of both the northern and southern pit walls in St. Margarethen gave almost identical but geologically meaningless results, because the constructed detachments do not flatten at depth but have an U-shaped geometry (Fig. 6). The construction of the domain closest to the observed master fault results in a plausible initial flattening of the detachment segment in the next domain. However, the constructed detachment segments of all other domains record continuous steepening and dip in the opposite direction than the steep part of the exposed fault at the surface (i.e. towards ESE) resulting in the geologically meaningless U-shaped fault geometry. We therefore conclude that the assumption of a rigid listric fault plane for the normal fault in St. Margarethen might be incorrect and other mechanisms were responsible for forming a hanging wall anticline.

Discussion

Listric versus planar fault geometry

Since both concepts of fault-related deformation, i.e. a rollover anticline above a listric fault as well as reverse

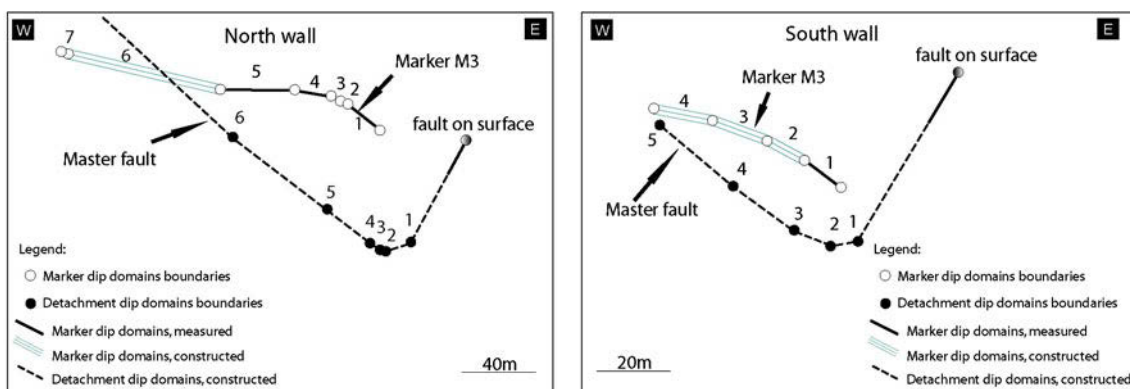


Fig. 6 Balanced cross-sections, **a** north wall and **b** south wall, using a dip domain technique in order to reconstruct the continuation of a listric fault at depth (Tearpock and Bischke 2003). We omitted a full-scale graphical reconstruction in order to avoid an abundance of auxiliary lines. The input parameters into the models are (1) the

spatial orientation of the marker bed M3 and (2) the true dip of the master fault at the hanging wall cut-off level. Both reconstructed sections do not result in a listric fault with a sub-horizontal detachment at depth but in geologically meaningless structures

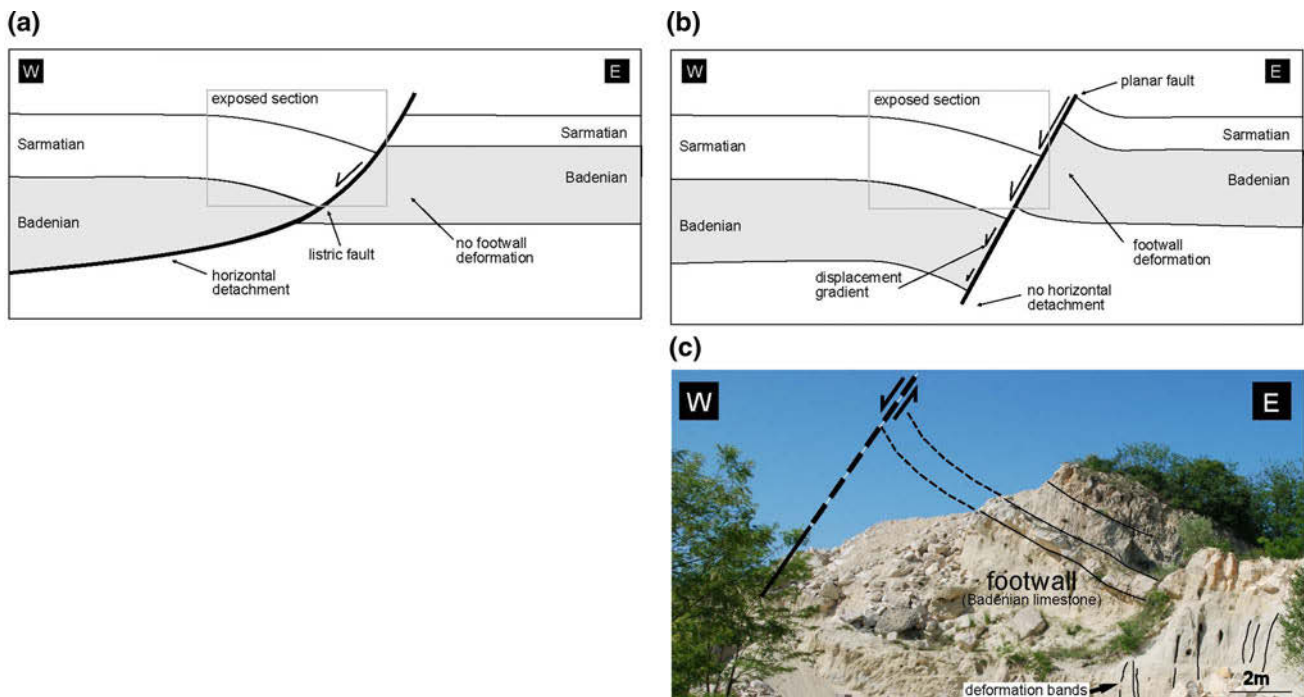


Fig. 7 Generalized cross-sections comparing the two conceptual models. **a** Listic fault model with constant displacement along a fault, which flattens at depth into a sub-horizontal detachment. The hanging wall is deformed into a rollover anticline, but there is no deformation within the footwall. **b** Model of a planar fault of finite length recording a displacement gradient. Fault movement induced perturbation strain that causes reverse drag in the hanging wall and in

the footwall. The exposed section in St. Margarethen records nearly identical geometry that characterizes the both models. **c** Outcrop picture of the Oslip quarry (location marked in Fig. 1) in a footwall position along the N–S trending fault system, exposing Badenian limestone and sand layers dipping to the E with ca. 40°, which is interpreted as reverse drag and associated deformation bands in the footwall of the normal fault

drag in the hanging wall of a planar fault, result in similar finite geometries, their respective applicability to the studied outcrop is discussed in the following section. Importantly, this study is restricted to mechanical models of anticlines related to normal faults and does not consider hanging wall anticlines occurring along inverted normal faults related to a compressional reactivation with thrust kinematics (e.g. McClay 1995).

Balancing techniques of listric faults are based on the concept of the displacement of the hanging wall along a curved fault surface, separating the deformable sedimentary pile in the hanging wall from an undeformable footwall (Fig. 7a). In these models, the shape of the fault largely controls the deformed geometry of the hanging wall. The success of the model of listric faults is largely based on the highly intuitive results of sandbox models (e.g. McClay 1990; McClay and Scott 1991), which result in geometries directly comparable to interpreted extensional faults from seismic sections (e.g. Bally 1983; Butler 2009). Since listric faults and associated hanging wall anticlines are common targets for hydrocarbon exploration, the balancing methods like the technique applied in this study have been widely used in order to support seismic interpretations (e.g. Gibbs 1984; Williams and Vann 1987).

In order to increase the fit between observations and models, numerous modifications of the model and the balancing technique have been suggested (for a review see Tearpock and Bischke 2003; Yamada and McClay 2003), some of which even imply deformation of the footwall (e.g. Koyi and Skelton 2001; Imber et al. 2003; Krézsek et al. 2007). Our simple restoration of the extensional fault in St. Margarethen does not result in a geologically plausible sub-horizontal lower part of a listric fault. The applied method is based on the assumptions of listric fault models but the constructed results are geologically meaningless and therefore we conclude that extension and hanging wall deformation were controlled by a different mechanical process.

A completely different group of models explain rollover structures (Fig. 7b), also referred to as reverse drag (Hamblin 1965), by displacement gradients along the fault (e.g. Barnett et al. 1987; Watterson et al. 1998). These models account for the frequent observation that a fault of finite length records lateral and vertical variations in displacement magnitude (e.g. Mansfield and Cartwright 2000). Such a displacement gradient induces wall-rock strains eventually leading to a bending, i.e. reverse drag, of markers at a high angle to the fault plane (Grasemann et al.

2005). The faults in these models are planar and not listric, and even slip gradients along “anti-listric” faults may often result in reverse drag (Reches and Eidelman 1995). If such a displacement gradient model is applied to the studied outcrop in St. Margarethen, the reverse drag observed in the hanging wall Sarmatian sediments may alternatively be explained by a slip gradient along a planar master fault. The deformation in the Sarmatian sediments is accommodated by secondary faults and deformation bands of finite length, which themselves record a displacement gradient and associated smaller scaled reverse drag (Exner and Grasemann 2010). Because the master fault exposed in the gravel pit of St. Margarethen cannot be traced further to the S across the Austrian-Hungarian border, where there is no evidence of extension in the Sarmatian/Pannonian sediments, a slip gradient on the master faults is geologically highly plausible. Displacement gradient as the primary mechanism for the drag in the Sarmatian sediments is furthermore supported by the GPR data and the integrated 3D structural model (Fig. 5), which show that the magnitude of the drag of marker horizons is changing along the strike of the master fault. Although the displacement gradient models predict fault drag in the hanging and the footwall, the magnitude and sense is strongly dependent on the exposed part of the fault and theoretically can juxtapose reverse drag in the hanging wall with normal or no drag in the footwall (Barnett et al. 1987; Grasemann et al. 2005). Unfortunately, the footwall in the quarry in St. Margarethen is not exposed. However, in direct continuation along the strike of the normal fault system to the N (Fig. 1, quarry Oslip), the Badenian sediments in the footwall of the master fault are strongly deformed by the formation of deformation bands and record a dip of 30° towards the W (Fig. 7c). We interpret that this tilt of the Badenian sediments below the master fault represents the footwall reverse drag. Based on the regional geological map, the dip variations of the Badenian sediments are clearly related to the faulting and therefore favour models that predict footwall deformation.

Hydrocarbon traps

The occurrence of hydrocarbon-trapping listric fault systems has been of great interest for oil and gas exploration around the world (e.g. Dula 1991; Nunns 1991; Withjack et al. 1995; Desheng 1996; Rowan et al. 1998; Bhattacharaya and Davies 2001; Dutton et al. 2004). Rollover anticlines are the least risky traps for petroleum depending on the juxtaposition of a shale seal across the fault plane (Allen and Allen 2005). The fault plane itself may or may not seal, allowing either lateral or vertical migration to higher structural levels (Weber 1978). However, detailed sub-surface mapping of listric faults frequently extends

below the level of coherent seismic data decreasing the reliability of interpretation. Furthermore, it has been shown that flattening normal faults are disappearing in the seismic data with increasing depth (“downwards dying growth faults”, e.g. Tearpock and Bischke 2003). Consequently, refined balanced cross-section techniques (see recent review by Poblet and Bulnes 2005), analogue (e.g. Vendeville and Cobbold 1988; Gaullier et al. 1993; Mauduit and Brun 1998) and numerical (Erickson et al. 2001 and references cited therein) models have been used in order to aid seismic interpretations. Especially, mechanical models introducing interaction between a newly formed steep normal fault and a pre-existing ductile low-angle detachment layer have increased the knowledge about plausible rheological and geometrical settings for normal faults, which flatten at depth. However, it is important to note that a large number of models that introduce ductile layers are strictly speaking not listric faults *sensu strictu* but can be better explained by a raft tectonic model, which is based on mechanical instabilities (Mauduit and Brun 1998).

Here, we argue that planar faults recording a displacement gradient may result in similar geometries as listric faults with rollover anticlines. This model is especially attractive, where (1) the fault records a high-angle relationship with the marker layers, (2) the fault cuts rocks of similar material behaviour in the hanging wall and in the footwall, (3) the fault has a finite length and records a displacement gradient and (4) no ductile layer (e.g. salt) is present at depth. An exceptional illustrative example has been investigated by a detailed 3D seismic interpretation of extensional faults in the Leona field in the Eastern Venezuela Basin (Porrás et al. 2003). In this interpretation, the major oil accumulations are confined to seals forming normal and reverse drag folds along faults with displacement gradients. Normal-drag folds form the largest traps, with extended reservoirs in the footwall of master normal faults, whereas reverse-drag folds provide the structural closure for trapping in the hanging wall.

Conclusions

We created a 3D structural model of deformed Sarmatian and Pannonian Sediments in the hanging wall of a normal fault bordering the eastern margin of the Eisenstadt-Sopron Basin. Spatial field measurements of faults and sedimentary layering, a terrestrial laser scan of an outcrop wall and GPR data behind the outcrop wall were integrated into the structural model. The dip of the sediments increases towards the west-dipping master fault resembling a roll-over structure above a listric normal fault. However, balanced cross-sections based on standard dip domain

techniques used for construction of listric faults do not result in geologically plausible structures. Considering the absence of a ductile horizontal layer at depth and the fact that the master fault terminates along strike towards the S, we argue that the observed reverse drag in the sediments is related to a slip gradient along a planar normal fault of finite length.

Acknowledgments This study was funded by the Austrian Science Fund (FWF-Project P20092-N10). We thank K. Decker, M. Wagneich and M. Harzhauser for discussion and providing information about earlier exposure conditions of the gravel pit.

References

- Allen PA, Allen JR (2005) Basin analysis: principles and applications. Wiley-Blackwell, London, pp 560
- Bally AW (1983) Seismic expression of structural styles. A picture and work atlas (3 vols). Am Ass Petrol Geol Stud Geol 15
- Barnett JAM, Mortimer J, Rippon JH, Walsh JJ, Watterson J (1987) Displacement geometry in the volume containing a single normal fault. Am Assoc Petr Geol B 71:925–937
- Bhattacharaya JP, Davies RK (2001) Growth faults at the prodelta to delta-front transition, Cretaceous Ferron sandstone. Utah Mar Petrol Geol 18:525–534
- Bristow CS, Jol HM (2003) An introduction to ground penetrating radar (GPR) in sediments. In: Bristow CS, Jol HM (eds) Ground penetrating radar in sediments. Geological Society of London Special Publications, vol 211, pp 1–7
- Brun JP, Mauduit TP-O (2008) Rollover in salt tectonics: the inadequacy of the listric fault model. Tectonophysics 457:1–11
- Brun JP, Mauduit TP-O (2009) Salt rollers: structure and kinematics from analogue modelling. Mar Petrol Geol 26:249–258
- Butler R (2009) Apulian foreland, offshore SE Italy. Virt Seis Atl Chamberlin RT (1910) The Appalachian folds of central Pennsylvania. J Geol 18:228–251
- Chwatal W, Decker K, Roch K-H (2005) Mapping active capable faults by high-resolution geo-physical methods: examples from the central Vienna basin. Aust J Earth Sci 97:52–59
- Crook AJL, Wilson SM, Yu JG, Owen DRJ (2006) Predictive modeling of structure evolution in sandbox experiments. J Struct Geol 28:729–744
- Davison I (1986) Listric normal fault profiles: calculation using bed-length balance and fault displacement. J Struct Geol 8:209–210
- Decker K (1996) Miocene tectonics at the Alpine-Carpathian junction and the evolution of the Vienna Basin. Mitt Ges Geol Bergbaustud Österr 41:33–44
- Decker K, Peresson H (1996) Rollover and hanging-wall collapse during Sarmatian/Pannonian synsedimentary extension in the Eisenstadt Basin. Mitt Ges Geol Bergbaustud Österr 41:45–52
- Decker K, Peresson H, Hinsch R (2005) Active tectonics and Quaternary basin formation along the Vienna Basin Transform fault. Quat Sci Rev 24:305–320
- Desheng L (1996) Basic characteristics of oil and gas basins in China. J Southe Asian Earth 13:299–304
- Dooley T, McClay K, Pascoe R (2003) 3D analogue models of variable displacement extensional faults: application to Revfallet Fault system off shore mid Norway. In Nieuwland DA (ed) New insights into structural interpretation and modelling. Geological Society of London Special Publications, vol 212, pp 151–167
- Dula WF (1991) Geometric models of listric normal faults and rollover folds. Am Assoc Petr Geol B 75:1609–1625
- Dutton DM, Lister D, Trudgill BD, Pedro K (2004) Three-dimensional geometry and displacement configuration of a fault array from a raft system, Lower Congo, Offshore Angola: implications for the Neogene turbidite play. In: Davies RJ, Cartwright JA, Stewart SA, Lappin M, Underhill JR (eds) 3D seismic technology: application to the exploration of sedimentary basins. Geological Society of London Mem., vol 29, pp 133–142
- Erickson SG, Strayer LM, Suppe J (2001) Mechanics of extension and inversion in the hanging walls of listric normal faults. J Geophys Res 106:26655–26670
- Exner U, Grasemann B (2010) Displacement gradients and heterogeneous strain along deformation bands in gravels. J Geol Soc Lond
- Fodor L (1995) From transpression to transtension: Oligocene-Miocene structural evolution of the Vienna Basin and the East Alpine-Western Carpathian junction. Tectonophysics 242:151–182
- Gaullier V, Brun JP, Guérin G, Lecanu H (1993) Raft tectonics: the effects of residual topography below a salt décollement. Tectonophysics 228:363–381
- Ge H, Jackson PAM, Vendeville B (1997) Kinematics and dynamics of salt tectonics driven by progradation. Am Assoc Petr Geol B 81:398–423
- Gibbs AD (1984) Structural evolution of extensional basin margins. J Geol Soc Lond 141:609–620
- Gibson JR, Walsh JJ, Watterson J (1989) Modelling of bed contours and cross-sections adjacent to planar normal faults. J Struct Geol 11:317–328
- Grasemann B, Martel S, Passchier CW (2005) Reverse and normal drag along a fault. J Struct Geol 27:999–1010
- Gupta A, Scholz CH (1998) A model of normal fault interaction based on observations and theory. J Struct Geol 22:865–879
- Hamblin WK (1965) Origin of “reverse drag” on the down-thrown side of normal faults. Geol Soc Am Bull 76:1145–1164
- Harzhauser M, Kowalke T (2002) Sarmatian (Late Middle Miocene) Gastropod Assemblages of the Central Paratethys. Facies 46:57–82
- Hinsch R, Decker K, Wagneich M (2005) 3-D mapping of segmented active faults in the southern Vienna Basin. Quat Sci Rev 24:321–336
- Imber J, Childs C, Nell PAR, Walsh JJ, Hodgetts D, Flint S (2003) Hanging wall fault kinematics and footwall collapse in listric growth fault systems. J Struct Geol 25:197–208
- Koyi HA, Skelton A (2001) Centrifuge modelling of the evolution of low-angle detachment faults from high-angle normal faults. J Struct Geol 23:1179–1185
- Krészsek C, Adam J, Grujic D (2007) Mechanics of fault and expulsion rollover systems developed on passive margins detached on salt: insights from analogue modelling and optical strain monitoring. In: Jolley SJ, Barr D, Walsh JJ, Knipe RJ (eds) Structurally complex reservoirs. Geological Society of London Special Publications, vol 292, pp 103–121
- Mansfield CS, Cartwright JA (2000) Stratal fold patterns adjacent to normal faults: observations from the Gulf of Mexico. In: Cosgrove JW, Ameen MS (eds) Forced folds and fractures. Geological Society of London Special Publications, vol 169, pp 115–128
- Mauduit T, Brun JP (1998) Development of growth fault/rollover systems: birth, growth, and decay. J Geophys Res 103:18119–18136
- McCaffrey KJW, Jones RR, Holdsworth RE, Wilson RW, Clegg P, Imber J, Holliman N, Trinks I (2005) Unlocking the spatial dimension: digital technologies and the future of geoscience fieldwork. J Geol Soc Lond 162:927–938
- McClay KR (1990) Extensional fault systems in sedimentary basins: a review of analogue model studies. Mar Petrol Geol 7:206–233

- McClay KR (1995) The geometries and kinematics of inverted fault systems; a review of analogue model studies. In Buchanan JG, Buchanan PG (eds) Basin inversion. Geological Society of London Special Publications, vol 88, pp 97–118
- McClay KR, Scott AD (1991) Experimental models of hanging wall deformation in ramp-flat listric extensional fault systems. *Tectonophysics* 188:85–96
- Meschede M, Aspöck U, Reicherter K (1997) Visualization of tectonic structures in shallow-depth high resolution ground-penetrating radar (GPR) profiles. *Terra Nova* 9:167–170
- Nunns AG (1991) Structural restoration of seismic and geologic sections in extensional regimes. *Am Assoc Petr Geol B* 75:278–297
- Poblet JBM, Bulnes M (2005) Fault slip, bed-length and area variations in experimental rollover anticlines over listric normal faults: influence in extension and depth to detachment estimations. *Tectonophysics* 396:97–117
- Porras JS, Vallejo EL, Marchal D, Selva C (2003) Extensional folding in the Eastern Venezuela Basin: examples from fields of Oritupano-Leona Block. *Search and Discovery Article #50003:7*
- Ratschbacher L, Frisch W, Linzer H-G, Merle O (1991) Lateral extrusion in the Eastern Alps: 2, structural analysis. *Tectonics* 10:257–271
- Reches Z, Eidelman A (1995) Drag along faults. *Tectonophysics* 247:145–156
- Reiss S, Reicherter KR, Reutner C-D (2003) Visualization and characterization of active normal faults and associated sediments by high-resolution GPR. In: Bristow CS, Jol HM (eds) Ground penetrating radar in sediments. Geological Society of London Special Publications, vol 211, pp 247–255
- Rowan MG, Hart BS, Nelson S, Flemings PB, Trudgill BD (1998) Three-dimensional geometry and evolution of salt related growth-fault array: Eudene Island 330 field, offshore Louisiana, Gulf of Mexico. *Mar Petrol Geol* 15:309–328
- Royden LH (1985) The Vienna Basin: a thin-skinned pull-apart basin. In: Biddle KT, Christie-Blick N (eds) Strike-slip deformation, basin formation, and sedimentation. *SEPM Special Publications*, vol 37, pp 319–338
- Schmid HP, Harzhauser M, Kroh A (2001) Hypoxic events on a middle miocene carbonate platform of the Central Paratethys (Austria, Badenian, 14 Ma). *Ann Naturhist Mus Wien* 102A: 1–50
- Shelton WJ (1984) Listric normal faults, an illustrated summary. *Am Assoc Petrol Geol Bull* 68:801–815
- Strauss P, Harzhauser M, Hinsch R, Wagreich M (2006) Sequence stratigraphy in a classic pull-apart basin (Neogene, Vienna Basin). A 3D seismic based integrated approach. *Geol Carpath* 57:185–197
- Suess E (1909) *Das Antlitz der Erde*. Tempsky F, Freitag G, Prag and Wien, Leipzig
- Tearpock DJ, Bischke RE (2003) Applied subsurface geological mapping, pp 821
- Vendeville B, Cobbold PR (1988) How normal faulting and sedimentation interact to produce listric fault profiles and stratigraphic wedges. *J Struct Geol* 10:649–659
- Wagreich M (2000) A slope-apron succession filling a piggyback basin the Tannheim and Losenstein Formations (Aptian–Cenomanian) of the eastern part of the North Calcareous Alps (Austria). *Mitt Österr Geol Ges* 93:31–54
- Watterson J, Nicol A, Walsh JJ (1998) Strains at the synchronous conjugate normal faults. *J Struct Geol* 20:363–370
- Weber KJ (1978) Hydrocarbon distribution patterns in Nigerian growth fault structures controlled by structural style and stratigraphy. *J Petrol Sci Eng* 1:91–104
- Wernicke B, Burchfiel BC (1982) Modes of extensional tectonics. *J Struct Geol* 4:105–115
- Wessely G (1988) Structure and development of the Vienna basin in Austria. In: Royden LH, Horváth F (eds) *Am Assoc Petr Geol B*, vol 45, pp 333–346
- Wheeler J (1987) Variable-heave models of deformation above listric normal faults: the importance of area conservation. *J Struct Geol* 9:1047–1049
- White N (1992) A method for automatically determining normal fault geometry at depth. *J Geophys Res* 97:1715–1733
- White NJ, Jackson JA, McKenzie DP (1986) The relationship between the geometry of normal faults and that of the sedimentary layers in their hanging walls. *J Struct Geol* 8:897–909
- Williams G, Vann I (1987) The geometry of listric normal faults and deformation in their hanging walls. *J Struct Geol* 9:789–795
- Withjack MO, Islam QT, La Pointe PR (1995) Normal faults and their hanging-wall deformation; an experimental study. *Am Assoc Petr Geol B* 79:1–18
- Xiao H, Suppe J (1992) Origin of rollover. *Am Assoc Petrol Geol Bull* 76:509–529
- Yamada Y, McClay K (2003) Application of geometric models to inverted listric fault systems in sandbox experiments. Paper 1: 2D hanging wall deformation and section restoration. *J Struct Geol* 25:1551–1560